ACS APPLIED MATERIALS & INTERFACES

Research Article

www.acsami.org

Simultaneous Reinforcing and Toughening of Polyurethane via Grafting on the Surface of Microfibrillated Cellulose

Xuelin Yao, Xiaodong Qi, Yuling He, Dongsheng Tan, Feng Chen,* and Qiang Fu*

College of Polymer Science and Engineering, State Key Laboratory of Polymer Materials Engineering, Sichuan University, Chengdu 610065, China

Supporting Information

ABSTRACT: In the present work, a series of thermoplastic polyurethane (TPU)/microfibrillated cellulose (MFC) nanocomposites were successfully synthesized via in situ polymerization. TPU was covalently grafted onto the MFC by particular association with the hard segments, as evidenced by Fourier transform infrared spectroscopy, X-ray photoelectron spectroscopy, and thermogravimetric analysis. The adequate dispersion and network structure of MFC in the TPU matrix and the strong interfacial interaction through covalent grafting and hydrogen bonding between MFC and TPU resulted in significantly improved mechanical properties and thermostability of the prepared nanocomposites. The tensile strength and elongation-at-break of the nanocomposite containing only 1 wt % MFC were increased by 4.5-fold and 1.8-fold compared with that of neat TPU, respectively. It was also very interesting to find that the glass transition temperature (T_g) of TPU was decreased significantly with the introduction of MFC, indicating potential for low-temperature resistance applications. Most importantly, compared with TPU nanocomposites reinforced with other nanofillers, the TPU/MFC nanocomposites prepared in this work exhibited excellent transparency and higher reinforcing efficiency.

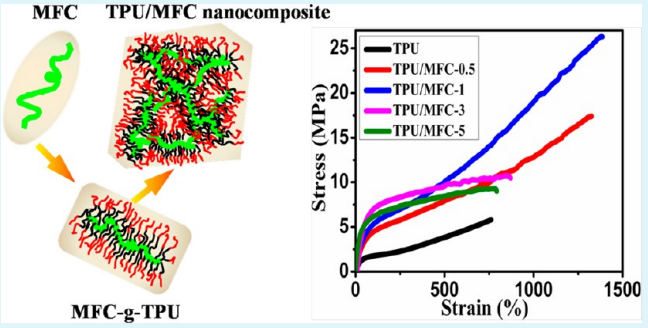

KEYWORDS: *thermoplastic polyurethane, microfibrillated cellulose, covalent grafting, high strength, high toughness*

1. INTRODUCTION

Recently, the introduction of nanoparticles/materials as reinforcement phases into polymer matrixes to form nanocomposites has attracted a great deal of attention because the composites can exhibit significantly improved mechanical properties even at quite low volume fraction. Typical reinforcement phases, such as hydroxyapatite,[1] clay,[2−6] carbon nanotubes,[7−10] and reduced graphene oxide,[11] have been studied extensively. However, most of these fillers are nonbiodegradable, which can bring tremendous pressure to very fragile ecological environments. In recent years, in order to reduce our dependence on oil resources to a certain degree, the proportion of materials from renewable resources has been increased through the use of natural plant fiber/polymer matrix composites.[12,13]

Cellulose fibrils displaying lateral dimensions on the nanometer scale and lengths on the micrometer scale can potentially serve as units for the construction of ideal strong and tough materials because of their semicrystalline structure of extended chains with small diameter as well as large aspect ratio (length/diameter), which is responsible for the intrinsically good mechanical properties.[13,14] These unique properties make this material a promising candidate as a sustainable polymer reinforcement material. Much research and attention has been focused on the isolation and production of nanocellulose, and for more detailed reviews of the production and application of nanocellose, the reader is referred to the publications by Siró and Plackett,[15] Klemm et al.,[16] and Moon et al.[13] An increasing number of studies found in the literature are focused on cellulose nanocrytals (CNCs; also called cellulose nanowhiskers), which have been incorporated into different matrixes as reinforcing agents.[17−25] These nanocelluloses are obtained from various resources (e.g., cotton, bleached wood pulp, bacteria, tunicin, etc.), often by means of an acid hydrolysis step for the digestion of amorphous cellulosic domains while leaving the crystalline regions intact;[26−28] after this treatment, individual and rodlike-shaped nanocelluloses are produced.

Unlike CNCs, microfibrillated cellulose (MFC; also called microfibrillar cellulose, microfibril cellulose, or nanofibril or fibril aggregates) consists of long, flexible, interconnected, and entangled cellulose nanofibers containing both crystalline and amorphous regions that are present as a complex network structure. Depending on the degree of fibrillation and any pretreatment involved, the dimensions and morphology of MFC vary considerably. Several different methods can be used to produce MFC, including enzymatic hydrolysis,[29] multipass high-pressure homogenization,[30] direct mechanical fibrillation,[31] or a combination of the aforementioned ways.[32]

Received: November 4, 2013
Accepted: January 29, 2014
Published: January 29, 2014

   dx.doi.org/10.1021/am4056694 | ACS Appl. Mater. Interfaces 2014, 6, 2497−2507

Through these methods, high-quality MFC now can be acquired by wood pulp fiber disintegration at a low cost. Furthermore, Isogai et al.[33] have prepared individualized cellulose nanofibers by 2,2,6,6-tetramethylpiperidine-1-oxyl radical (TEMPO)-mediated oxidation and done a lot of significant research on these materials. Compared to CNCs, MFC has a larger aspect ratio, and as a result of the relatively simple preparation process, it is also readily available and renewable, has a low density, and is easy to modify chemically.[34] Therefore, the use of MFC is very interesting and has allowed the creation of advanced and functional materials with hierarchical structures[35,36] as well as the development of cellulose-based materials with greater toughness,[37,38] better electrical and magnetic properties,[39−42] and higher optical transparency.[43,44] Incorporating MFC into polymers has also been shown to significantly improve the mechanical properties of the polymer. Lee et al.[45] impregnated MFC paper with an epoxy resin, and the cellulose-reinforced epoxy had a stiffness of ∼8 GPa and a strength of ∼100 MPa at a volume of 60%. MFC has already been incorporated into other different polymer matrixes, and this has proven to be an effective method to obtain nanocomposites with excellent performance.[46−51]

Thermoplastic polyurethane (TPU) has a copolymer structure with isocyanate and a chain extender (i.e., diol or diamine) as hard segments and polyether polyols or polyester polyols as soft segments. However, the thermodynamic incompatibility between the hard segments and the soft segments results in microphase separation. TPU is an interesting family of polymers since its elasticity modulus is between those of plastics and rubbers, allowing it to maintain good elasticity over a wide range of hardness.[52−57] TPU is quite a useful polymer for high-end medical, technological, and industrial applications. It has been used in a range of commodity products in the form of elastomers, foams, coatings, and adhesives. CNCs[58−60] and microcrystalline cellulose (MCC)[61] have been used as reinforcing fillers in TPU.

Currently, there are only a few reported works on TPU/MFC nanocomposites/composites,[62,63] since as a result of the complex entanglement and network structure of MFC, it is unlikely to disperse into individual fibrils. However, the appropriate entanglement and confined network structure of MFC can play an important role in reinforcement. We hypothesized that with adequate surface chemistry, MFC with its large aspect ratio and confined network structure could act as as reinforcing fiber and that its ability to unravel and bridge cracks could also aid in the toughening of TPU. Since van der Waals forces among the nanofibrils and their hydrophilic property hinder the dispersion and produce agglomerated morphologies, the main issues to address are adequate dispersion and a strong interfacial interaction between MFC and TPU, which are responsible for developing strong interfacial adhesion and enhancing the mechanical properties of the composite. Obviously, an effective and ideal way to achieve this purpose is through covalent attachment of TPU to the stiff surface of MFC by making the most of the abundant hydroxyl groups (−OH) on the surface of MFC. It is aimed at simultaneously reinforcing and toughening TPU by aptly adding MFC at very low loadings, ultimately benefiting the advancement of fabrication of large thermoplastic composites via reactive processing.

2. EXPERIMENTAL SECTION

2.1. Materials. *N*,*N*-Dimethylformamide (DMF) (Bodi Chemical Co., Ltd., Tianjin, China) was dehydrated by calcium hydride for 24 h stirring at room temperature and then redistilled under vacuum. 4,4′-Diphenylmethane diisocyanate (MDI) (Aladdin), poly(tetramethylene glycol) (PTMG) (M_n = 1000, Aldrich), and 1,4-butanediol (1,4-BD) were purified before use.

2.2. Preparation of Microfibrillated Cellulose. The cellulose material (Celish MFC KY100-S, Daicel Chemical Industries, Ltd., Japan), which was prepared from wood pulp by a number of homogenization processes, was used as reinforcement. The MFC contained water (solid content of 25%) in its initial state and was dried to constant weight at 70 °C before use. The dried solid MFC was first immersed in dehydrated DMF with stirring for 12 h to swell, and then the pretreated MFC was subjected to the homogenizing action of a high-speed shearing emulsification machine (FA25, Shanghai Sumai Trading Co., Ltd.). It should be noted that a longer shearing time may result in better dispersion but easier degradation of MFC because the high-speed shearing process can produce large amounts of heat. One may wonder whether drying the cellulose material directly from water could further promote aggregation of the cellulose fibers. Therefore, we checked the dispersion of MFC after it was dissolved in DMF, and the results are shown in Figure S1 in the Supporting Information. As can be seen, both the as-received MFC and the dried MFC present complex nanofiber aggregation and a weblike structure. The diameter of the cellulose fibers for the dried MFC was somewhat bigger. Since the basic idea of this work is to introduce chemical grafting between TPU and cellulose fibers, the slightly increased aggregation can be ignored.

2.3. Preparation of TPU/MFC Nanocomposite Films. The TPU prepolymer was synthesized by reacting MDI with PTMG (M_n = 1000) in DMF at 80 °C with mechanical stirring under a dry nitrogen atmosphere for 2 h. Then the desired amount of MFC suspended in DMF was added, and the reaction was allowed to continue for another 1 h. Subsequently, the chain extender 1,4-BD was added to the prepolymer and reacted for 1 h. The product was degassed by rotary vacuum evaporation at room temperature and then cast in a Teflon mold at 70 °C for 24 h to obtain a transparent film with a thickness of about 200 μm. In order to remove the DMF residues, the film was treated at 80 °C under vacuum for another 48 h. The amount of reactive hydroxyl groups on the MFC was 1.248 mmol/g as measured by using a titration to determine the excess isocyanate groups after mixing of MFC with a given amount of MDI. The molar ratio of MDI to PTMG in the prepolymer was 2:1, and the total NCO/OH ratio in the TPU was equal to 1. By changing the loading of MFC from 0 to 0.5, 1, 3, or 5 wt % and the amount of 1,4-BD, a series of transparent TPU nanocomposite films were successfully prepared, coded as TPU, TPU/MFC-0.5, TPU/MFC-1, TPU/MFC-3, and TPU/MFC-5, respectively. In order to investigate the interactions between TPU and the MFC surface, the resulting films were subjected to Soxhlet extraction using acetone for 48 h to separate the MFC from the physically absorbed polymer. The residue was made into a film and dried at 80 °C under vacuum for 24 h and then weighed and further characterized.

2.4. Characterization. *2.4.1. Fourier Transform Infrared Analyses.* FTIR spectroscopy was performed on Nicolet FTIR spectrometer (Nicolet FTIR 6700, Thermo Electron Co., USA) at room temperature. A film obtained by casting a suspension of unmodified MFC in a glass dish at 70 °C for 48 h, the film of modified MFC obtained after the Soxhlet extraction procedure, and the TPU/MFC nanocomposite films were characterized. The data were collected from 4000 to 400 cm^{-1} with a resolution of 4 cm^{-1} under reflection mode.

2.4.2. X-ray Photoelectron Spectroscopy. In order to demonstrate the change in functional groups on the surface of MFC and any variation in the carbon/oxygen ratio, X-ray photoelectron spectroscopy (XPS) experiments using an Axis Ultra DLD spectrometer (Kratos Co., UK) were performed on the dried MFC films before and after

reaction using focused monochromatized Al Kα radiation (15 kV) at room temperature.

2.4.3. Scanning Electron Microscopy. The cross-section morphologies of nanocomposite films were examined by scanning electron microscopy (SEM) using a JEOL JSM-5900LV scanning electron microscope at an accelerating voltage of 20 kV. Surfaces cryofractured using liquid nitrogen and fractured surfaces after tensile testing were investigated.

2.4.4. Thermogravimetric Analysis. Thermogravimetric analysis (TGA) was performed on a Q500 analyzer (TA Instruments) under a nitrogen atmosphere. The samples were heated from 25 to 600 °C at a heating rate of 10 °C/min. For each thermogravimetric analysis, around 10 mg of sample was used.

2.4.5. UV–Vis Spectroscopy. The UV–vis spectra were recorded on a UV-1800PC spectrophotometer at room temperature, and the data were collected from 450 to 650 nm. The thickness of the neat TPU and TPU/MFC nanocomposite films was about 200 μm. The films were dried at 80 °C under vacuum for 12 h to remove the absorbed moisture before testing.

2.4.6. Measurements of Mechanical Properties. 2.4.6.1. Dynamic Mechanical Analysis. The dynamic mechanical properties of the TPU/MFC films were measured using a dynamic mechanical analyzer (DMA Q800, TA Instruments) in tension mode at a frequency of 1 Hz and a heating rate of 3 °C/min over the temperature range from −100 to 100 °C. The samples were prepared by cutting 7 mm wide strips from the films.

2.4.6.2. Tensile Measurements. The tensile measurements were carried out on an Instron 5567 Universal Testing Machine at room temperature with a gauge length of 20 mm and a crosshead speed of 50 mm/min. The reported values were calculated as averages over five replicates for each sample.

3. RESULTS AND DISCUSSION

3.1. Grafting of TPU on the Surface of MFC. The morphology of MFC treated by homogenization processes for 10 min was characterized by SEM, as shown in Figure 1a. It can be seen that MFC exhibited a complex and weblike structure after the emulsification process. Diameters ranging from 40 to 100 nm can be identified from the micrograph; however, it was hard to measure the length and diameter of each MFC with high accuracy because of the complex network morphology.

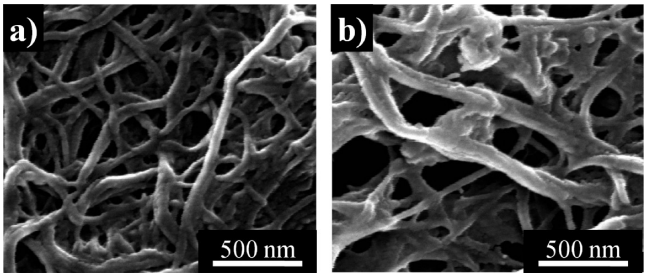

Figure 1. SEM images of (a) MFC after homogenization using the emulsification machine and (b) the residue obtained from the TPU/MFC-3 nanocomposite (IMFC-3) after the Soxhlet extraction process.

The preparation of TPU/MFC nanocomposites was carried out via addition polymerization of isocyanate on the ends of the TPU prepolymer with hydroxyl groups on the MFC surface, as represented in Scheme 1. During the process of polymerization of TPU, different amounts of MFC were introduced. In order to confirm that the TPU chains were successfully grafted on MFC and determine the amount of grafted polymer, the obtained TPU/MFC films were subjected to a Soxhlet extraction process. The residues were dried to constant weight and analyzed. In general, after the Soxhlet extraction process, the physically absorbed TPU on MFC was dissolved in acetone and easily removed, leaving only the TPU covalently linked to MFC. Figure 1b shows the morphology of IMFC-3 obtained by performing the Soxhlet extraction procedure on a sample of the TPU/MFC-3 composite to dissolve and remove the physically absorbed TPU on MFC. A larger width compared with that in the original MFC obtained from a high-speed shearing emulsification process (Figure 1a) can be clearly recognized. MFC uniformly wrapped with TPU, primarily attributed to the contribution of the grafting of TPU on the surface of MFC, can be easily identified and was further confirmed by FTIR and XPS as described below. Table 1 reports the results of an analysis of the TPU grafts that were covalently attached to the MFC surface. It was found that the TPU content in the grafted MFC-*g*-TPU varied from 34 to 42 wt %, in which the amount of grafted TPU was calculated on the basis of the mass of MFC in the sample and the mass of the residue.

To further verify the possible interaction between TPU and MFC, FTIR spectroscopy was carried out on the residues from Soxhlet extraction. TPU/MFC-3 was taken as an example, and the spectra of IMFC-3, the original MFC, and neat TPU are shown in Figure 2. Comparison of the spectra of the original MFC and IMFC-3 reveals two new absorbance bands at 1706 and 1512 cm^{-1}, which can be ascribed to the absorption of carbonyl groups (C═O) and N−H bending combined with C−N asymmetric stretching, respectively, suggesting the possible reaction of hydroxyl groups (−OH) of cellulose with isocyanate (−NCO). The intensity of the peak located at 2852 cm^{-1} (corresponding to alkane C−H stretching vibrations) is increased, demonstrating that more $-CH_2-$ exists in the residues than in the MFC. This also confirms that the TPU molecule chains were successfully grafted on MFC.

XPS was also used to evaluate the chemical composition of the residues, especially to confirm the presence of TPU polymer on MFC after Soxhlet extraction. As shown in Figure 3, the low-resolution spectrum of the original MFC (Figure 3a) suggests that carbon and oxygen atoms are the main components, while the spectra of the residues (TPU/MFC-0.5 and TPU/MFC-5 are chosen for comparison) show that nitrogen atoms are present (Figure 3b,c), which can only be explained by the existence of urethane groups. In the high-resolution spectra for both the original MFC and the modified MFC residues (Figure 3 insets), the carbon peak was fit to three peaks that can be ascribed to carbon atoms in different local environments (C−C, C−O, and O−C−O), and different proportions of each type of carbon atom were obtained. After the TPU grafting reaction, the proportion of carbon atoms without oxygen linkages (C−C) increased significantly and that of carbon atoms with one band to oxygen (C−O) decreased (Figure 3b,c insets). The presence of TPU polymers grafted on the surface of MFC must be invoked to explain these phenomena.

Thus, from the combination of the results of the quality analysis of the Soxhlet extraction and the FTIR and XPS results it can be concluded that part of the TPU prepolymer terminated with isocyanate groups was successfully grafted on the surface of MFC by the reaction with hydroxyl groups on MFC.

One expects a strong interaction between the grafted MFC and the TPU matrix. FTIR once again was used to characterize the TPU/MFC nanocomposites instead of the residues after Soxhlet extraction, and the results are shown in Figure 4. Two new bands at 1708 and 1512 cm^{-1} can be seen in the spectra of

Scheme 1. Illustration of the in Situ Polymerization Process To Prepare TPU/MFC Nanocomposites

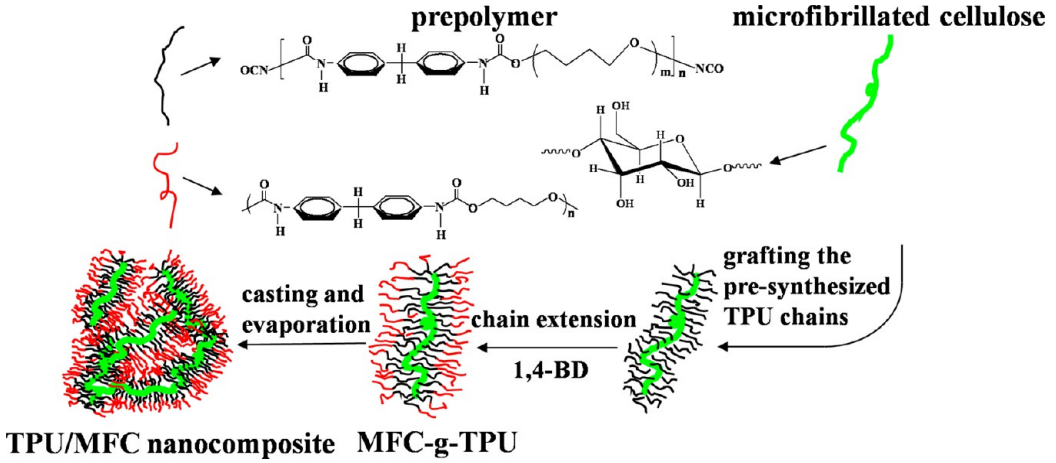

Table 1. Results of the Analyses of TPU/MFC Nanocomposites before and after Soxhlet Extraction

sample	TPU content (wt %)[a]	initial mass of the sample (g)	mass of MFC in the sample (g)	mass of residue (g)
TPU	0	2.473	0	0
TPU/MFC-0.5	38.68	1.854	0.009	0.015
TPU/MFC-1	42.27	2.083	0.021	0.036
TPU/MFC-3	36.19	3.401	0.102	0.160
TPU/MFC-5	34.31	2.150	0.108	0.164

[a]TPU content in the MFC-*g*-TPU sample based on the mass of MFC in the sample and the mass of the residue.

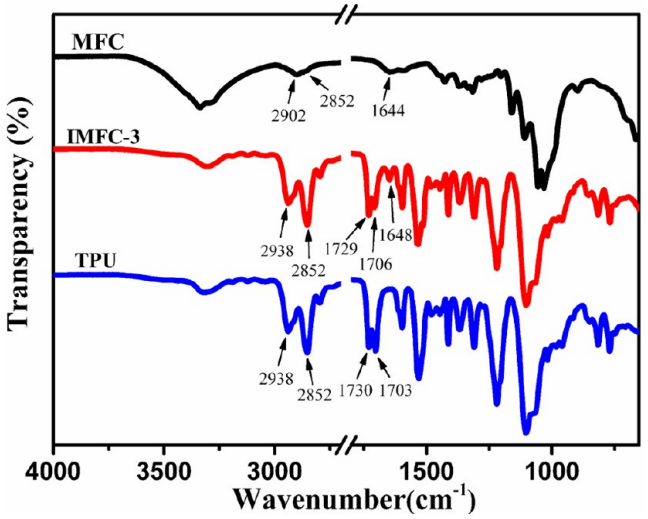

Figure 2. FTIR spectra of the original MFC, IMFC-3, and neat TPU.

the TPU/MFC nanocomposites (Figure 4a), which can be ascribed to the absorption of carbonyl groups (C═O) and N−H bending deformation combined with C−N asymmetric stretching, respectively, suggesting a possible reaction of isocyanate groups (−NCO) of TPU with hydroxyl groups (−OH) of cellulose. A band at 3350 cm^{-1} was observed for the TPU/MFC composites (Figure 4b), which can be ascribed to the absorption of the inner unreacted hydroxyl groups of MFC. For each curve in Figure 4b, there is a band located at around 3299 cm^{-1} corresponding to N−H stretching, and no band around 3500 cm^{-1} appears (bands at 3500 and 3320 cm^{-1} correspond to stretching of free and hydrogen-bonded N−H respectively,[52]), indicating that all of the N−H groups in the TPU nanocomposites could be hydrogen-bonded. It is well-known that the N−H stretching band is sensitive to hydrogen bonding. Compared with neat TPU, the N−H stretching peak of the TPU/MFC nanocomposites is shifted to a lower wavenumber, indicating the existence of hydrogen bonding between N−H groups in TPU molecular chains and hydroxyl groups on MFC. The absorbance bands located at 1730 and 1708 cm^{-1} are ascribed to splitting of the carbonyl absorption, corresponding to the free and hydrogen-bonded carbonyls. The carbonyl hydrogen-bonding index,[2] namely, the ratio of absorbance intensity of the hydrogen-bonded carbonyl to that of the free carbonyl, decreases with increasing MFC content, which means that the introduction of MFC hinders the formation of hydrogen bonding between the hard segments of TPU.

3.2. Dispersion of MFC in the TPU Matrix. The dispersion of MFC in the TPU matrix was evaluated by SEM. Figure 5 presents the SEM images of a cross-section of the unfilled TPU matrix and nanocomposite films filled with 1, 3, and 5 wt % MFC, respectively. Distinguished from the micrograph of unfilled TPU, the morphology of the MFC in the TPU matrix can easily be identified. The MFC appears as white dots whose density on the fracture surface of the nanocomposite increases proportionally with the loading of MFC and without any large agglomeration. In addition, as the white dots are distributed uniformly throughout the entire fracture surface for each nanocomposite, good dispersion of MFC in the TPU matrix can be deduced. The improved dispersion and compatibility between MFC and TPU can be attributed to covalent attachment of TPU molecules to the stiff surface of MFC, which is expected to play an important role in the performance of the prepared nanocomposites.

3.3. Thermal Properties of TPU/MFC Nanocomposites. The thermal degradation of polyurethane is a complex process that in general can be divided into two stages. The first stage is mainly attributed to the decomposition of the hard segments, including the dissociation of urethane to the original polyol and isocyanate, which then develops into a primary amine, an alkene, and carbon dioxide. The consequent stage is controlled by the mechanisms of depolycondensation and degradation of polyol and is influenced by the content of the soft segment.[2,64] TGA curves for the original MFC, neat TPU, and the TPU/

dx.doi.org/10.1021/am4056694 | ACS Appl. Mater. Interfaces 2014, 6, 2497−2507

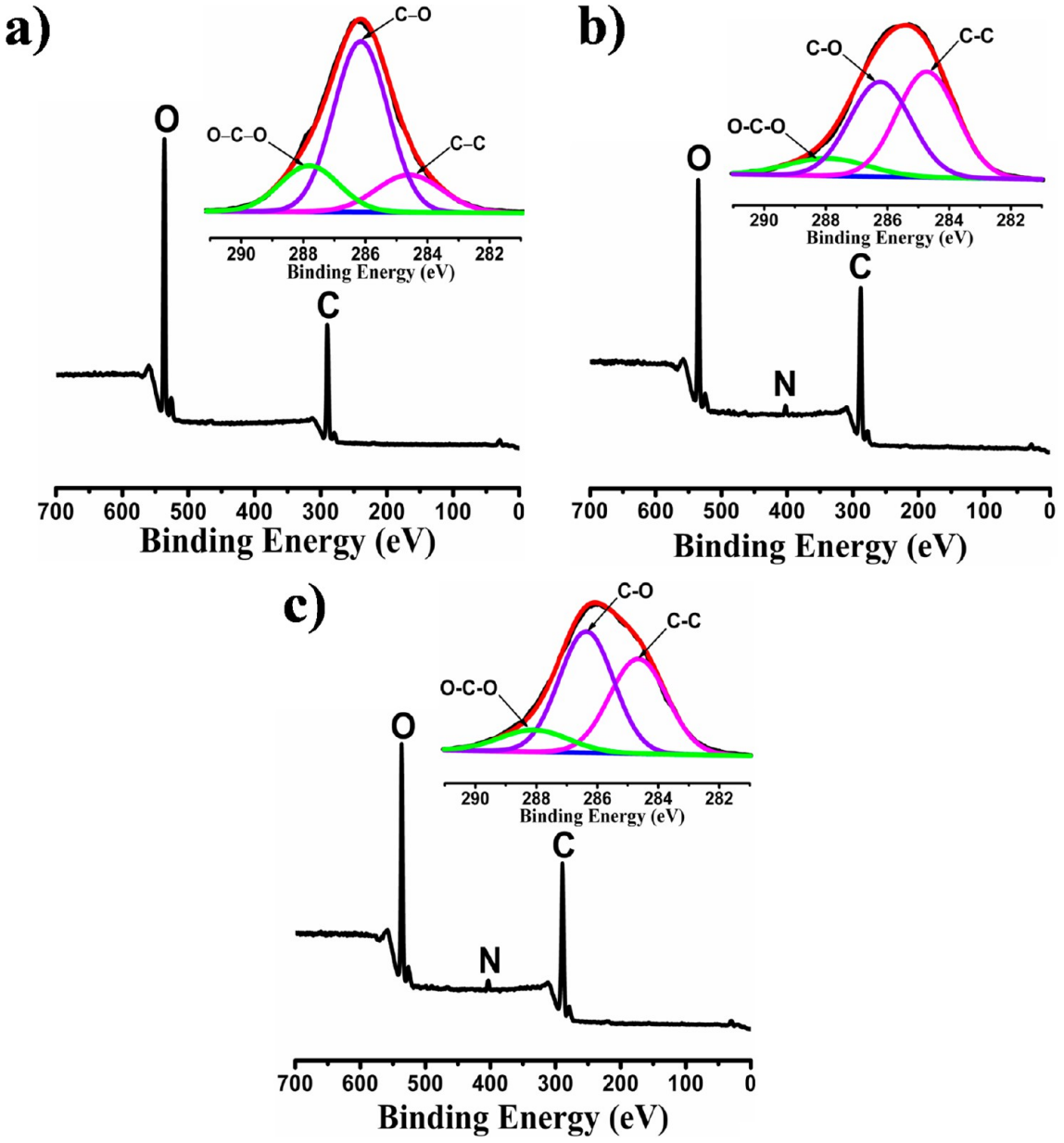

Figure 3. XPS spectra of MFC (a) before and (b, c) after the TPU grafting reaction and Soxhlet extraction process [(b) 0.5 wt % MFC; (c) 5 wt % MFC].

MFC nanocomposites with various loadings of MFC are shown in Figure 6. All of the thermal degradation curves can be divided into two stages except for that of the original MFC. The degradation of MFC starts at 220 °C, and the temperature with 5% weight loss of MFC ($T_{5\%}$) occurs at 304 °C. The first degradation of neat TPU occurs at 352 °C and the second degradation at 418 °C. It is very interesting to find that adding MFC (with a lower degradation temperature) into TPU causes a shift of in the first degradation temperature toward higher temperature (about 20 °C ahead). In other words, the first degradation temperature of TPU can be significantly improved by addition of MFC. Meanwhile, the second degradation temperature remains nearly constant, which demonstrates that the MFC is mainly associated with the hard segments in the TPU structure. These results further indicate that the MFC was successfully wrapped with TPU molecules by the reaction between the hydroxyl groups on the MFC surface and the TPU prepolymer. The improvement in the thermal stability of TPU due to the presence of MFC can be ascribed to the confined network structure and uniform dispersion of MFC in the TPU/MFC nanocomposites as well as a strong interfacial interaction between MFC and the TPU matrix through covalent attachment.

3.4. Mechanical Properties of TPU/MFC Nanocomposites. MFC is a kind of ideal filler for polymer reinforcement because of its large aspect ratio and excellent mechanical properties. In order to investigate the effect of MFC as a reinforcement phase in TPU nanocomposites, both dynamic mechanical analysis and classic tensile tests were applied. The effects of MFC on the thermomechanical properties of the TPU/MFC nanocomposites are shown in Figure 7. For the neat TPU, the storage modulus experiences a sharp decrease at its glass−rubber transition temperature (T_g), at around −35 °C, due to the thermoplastic nature of TPU. The modulus

dx.doi.org/10.1021/am4056694 | ACS Appl. Mater. Interfaces 2014, 6, 2497−2507

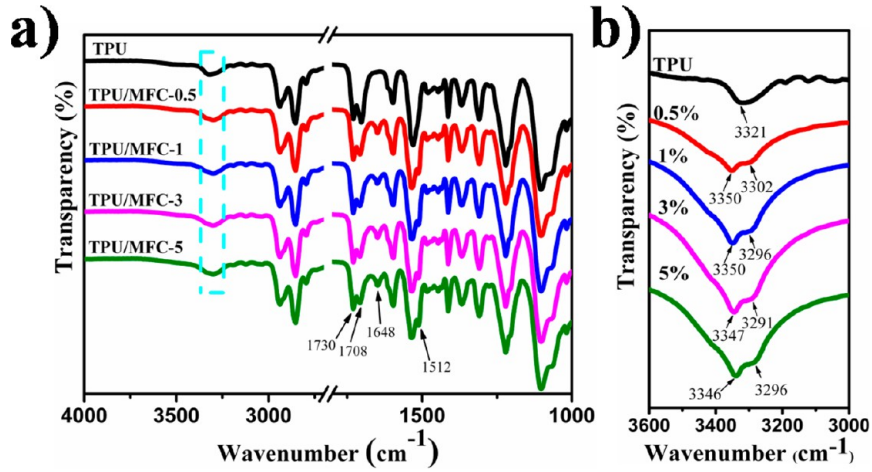

Figure 4. (a) FTIR spectra of neat TPU and TPU/MFC nanocomposites with different MFC loadings. (b) Amplified FTIR spectra of the circled region in (a).

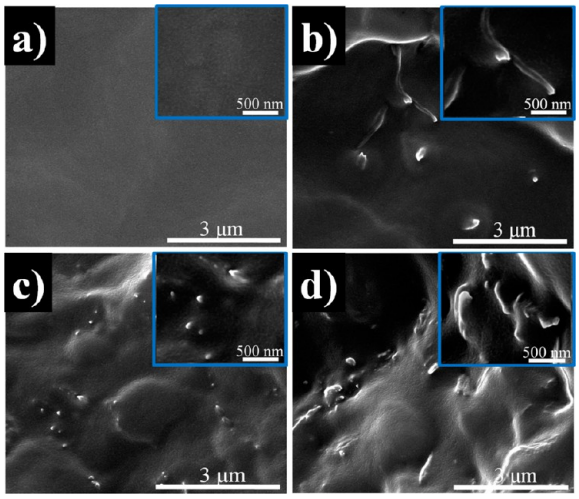

Figure 5. SEM images of the TPU/MFC nanocomposites with different MFC contents: (a) 0, (b) 1, (c) 3, and (d) 5 wt %.

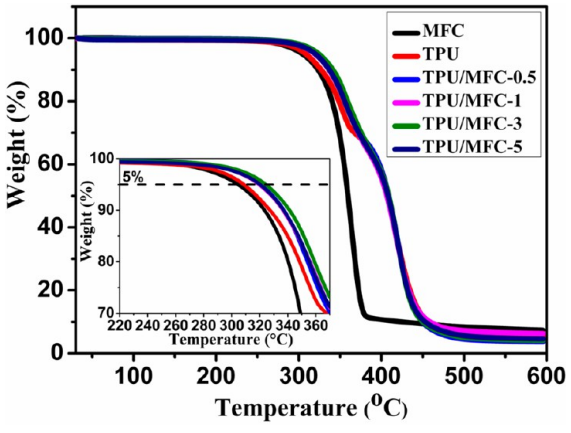

Figure 6. TGA curves of MFC, neat TPU, and the TPU/MFC nanocomposites with different MFC loadings.

continues to decline with increasing temperature down to zero at 60 °C. A remarkable improvement in the storage modulus is observed when MFC is introduced into the TPU matrix, particularly in the temperature range above T_g. For example, the modulus of the TPU/MFC nanocomposite with 1 wt % MFC loading is 180% and 1250% higher than that of neat TPU at temperatures of 20 and 50 °C, respectively, as shown in Figure 7a. This significant enhancement of rigidity due to the presence of MFC may be related to the confined network structure in the TPU/MFC nanocomposites as well as the strong adhesion force between the TPU matrix and MFC arising from the reaction between hydroxyl groups on the MFC surface and the TPU prepolymer, as demonstrated by the FTIR and TGA results. When the temperature is below T_g, the storage modulus of the TPU/MFC nanocomposites is slightly higher than that of neat TPU. However, one observes a shift of T_g toward even lower temperature (around −45 °C) for the TPU/MFC nanocomposites compared with neat TPU. This is a very important finding that will broaden the application of TPU in a lower temperature range as a thermoplastic elastomer. The decrease in the T_g of TPU upon addition of MFC can be more clearly demonstrated by the dependence of tan δ on temperature for TPU and the TPU/MFC nanocomposites, as shown in Figure 7b. The tan δ peak is associated with the T_g of the soft segment. Clearly, the addition of MFC results in a decrease in T_g (by around 10 °C) and the damping capacity. In this system, two effects must be taken into account. On one hand, the well-dispersed and confined network structure of MFC limits the molecular motion, causing an increase in T_g. On the other hand, the MFC is strongly associated with the hard segments of TPU and reduces the proportion of hydrogen-bonded carbonyls in the hard segments, as suggested by the FTIR results, resulting a more phase-separated structure between the hard segments and the soft phase and thus an increase in the chain mobility of the soft segments, which leads to a decrease in T_g. Obviously, the results indicate that the latter plays a more important role, resulting in the shift of T_g toward a lower temperature.

Figure 8 shows the stress−strain curves of neat TPU and the nanocomposites reinforced with different loadings of MFC. Compared with neat TPU, there is a remarkable increase in the initial stage of the stress−strain curve and an increase in tensile strength associated with increasing strain. The introduction of MFC as the reinforcing filler significantly improves the Young's modulus, tensile strength, and elongation-at-break, and the results are summarized in Table 2. It can be seen that the tensile strength increases from 5.8 ± 1.7 MPa for neat TPU to 17.4 ± 3.2 MPa for TPU/MFC-0.5 and further to 26.3 ± 3.7

dx.doi.org/10.1021/am4056694 | ACS Appl. Mater. Interfaces 2014, 6, 2497−2507

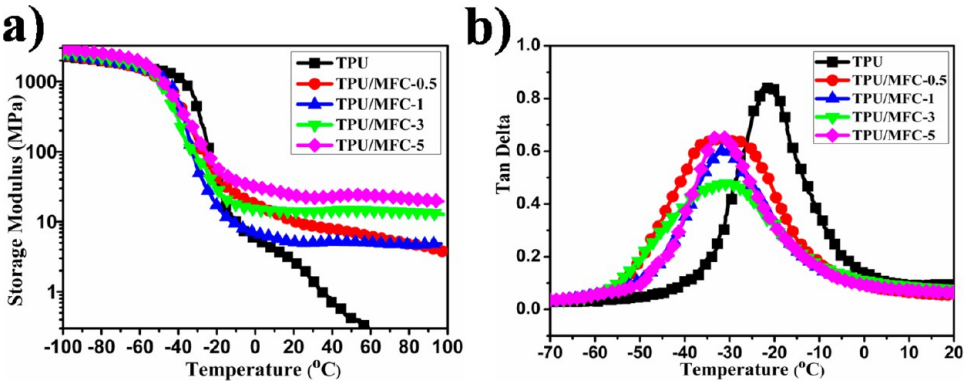

Figure 7. (a) Storage modulus of neat TPU and the TPU/MFC nanocomposites as a function of temperature. (b) Damping factor tan δ for neat TPU and the TPU/MFC nanocomposites as a function of temperature.

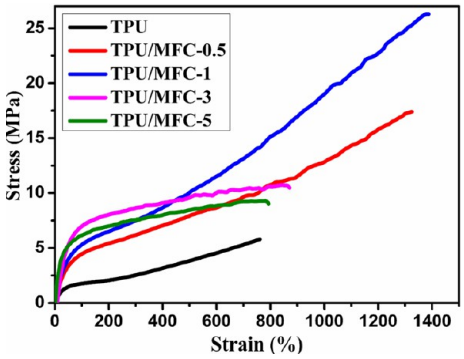

Figure 8. Stress–strain curves for TPU and TPU/MFC nanocomposite films with different MFC loadings.

Table 2. Mechanical Properties of Neat TPU and the TPU/MFC Nanocomposites Obtained from Tensile Tests: Young's Modulus (E), Tensile Strength (σ_B), and Elongation-at-Break (ε_B)

sample	E (MPa)	σ_B (MPa)	ε_B (%)
TPU	1.2 ± 0.2	5.8 ± 1.7	760.8 ± 33.8
TPU/MFC-0.5	5.4 ± 0.5	17.4 ± 3.2	1325.8 ± 46.5
TPU/MFC-1	7.1 ± 2.6	26.3 ± 3.7	1387.5 ± 57.2
TPU/MFC-3	20.6 ± 1.6	10.7 ± 0.1	871.7 ± 30.7
TPU/MFC-5	27.7 ± 1.3	9.3 ± 0.8	792.9 ± 25.9

MPa for TPU/MFC-1, where a more than 4-fold improvement has been achieved. The values of the elongation-at-break for the TPU/MFC nanocomposites increase in the range of 0–1 wt % MFC content, reaching the highest value of 1387.5 ± 57.2% for TPU/MFC-1, and then experiences a decrease when the MFC content is higher than 3 wt %. Thus, 1 wt % appears to be the optimal content. The Young's modulus increases with MFC content and reaches a maximum of 27.7 ± 1.3 MPa at 5 wt % MFC, which is more than 20 times higher than that of neat TPU (1.2 MPa). Typically, the introduction of rigid fillers into thermoplastic matrices provides enhancements in modulus and strength at the cost of a reduction in toughness due to a suppression of plastic deformation upon deformation and thus a decrease in elongation-at-break.[65−68] On the contrary, the TPU/MFC nanocomposites do not exhibit such a trend. Here we observe simultaneous reinforcing and toughening of polyurethane by addition of MFC. This can be ascribed to the TPU–cellulose interaction in the present materials due to the reaction between isocyanate and the cellulose hydroxyls, as the MFC also functions as a cross-linker with positive effects on the physical TPU network (increased effective cross-link density of the elastomer), whereas neat TPU does not contain a cross-linker. In addition, the existing network structure and homogeneous dispersion of MFC in the TPU matrix play important roles.

Figure 9 compares the values of the relative modulus (Figure 9a) and elongation-at-break (Figure 9b) as functions of filler content for TPU nanocomposites reinforced with MFC, CNCs,[60] MCC,[61] montmorillonite,[2] multiwalled carbon nanotubes (MWNTs) and single-walled carbon nanotubes (SWNTs),[10] laponite,[4] vermiculite,[5] and reduced graphene oxide (rGO).[11] The relative modulus is expressed as E/E_m, where E and E_m are the values of Young's modulus for the nanocomposite and the TPU matrix, respectively. Figure 9a clearly shows that MFC exhibits superior reinforcement effects on TPU matrix compared with the other nanofillers. For example, at a filler content of 1 wt %, the relative modulus of TPU/MFC is apparently higher than that of TPU/CNC and more than 5 times higher than those of the others. More notably, in Figure 9b, the elongation-at-break of TPU/MFC nanocomposite films is much higher than those of TPU reinforced by other fillers. The TPU nanocomposite film containing 1 wt % MFC shows the largest elongation-at-break (around 1400%) compared with the others, and a larger value is maintained even at higher MFC contents (around 870% and 800% for 3 and 5 wt % MFC, respectively). To the best our knowledge, the high reinforcement effect at such a low MFC content (only 1 wt %) while maintaining the great elongation-at-break at the same time has not been reported previously for any TPU matrix reinforced with nanoscale fillers.

3.5. Reinforcing Mechanism of TPU/MFC Nanocomposites. MFC is made up of long nanofibers that are entangled with each other and form a networklike structure, as can be seen in Figure 1. This unique structural characteristic may enhance load transfer between the MFC and the polymer matrix. At the same time, unraveling and splaying of the entangled fillers, together with the strong interaction between MFC and the TPU matrix through covalent attachment, may enable the MFC to bridge the polymer matrix during crack propagation, hence improving not only the stiffness but also the toughness of the nanocomposite.

In order to further investigate the reinforcing mechanism leading to the simultaneous enhancement in stiffness and toughness of TPU upon addition of MFC, the tensile fracture surfaces of neat TPU, TPU/MFC-1, and TPU/MFC-3 were

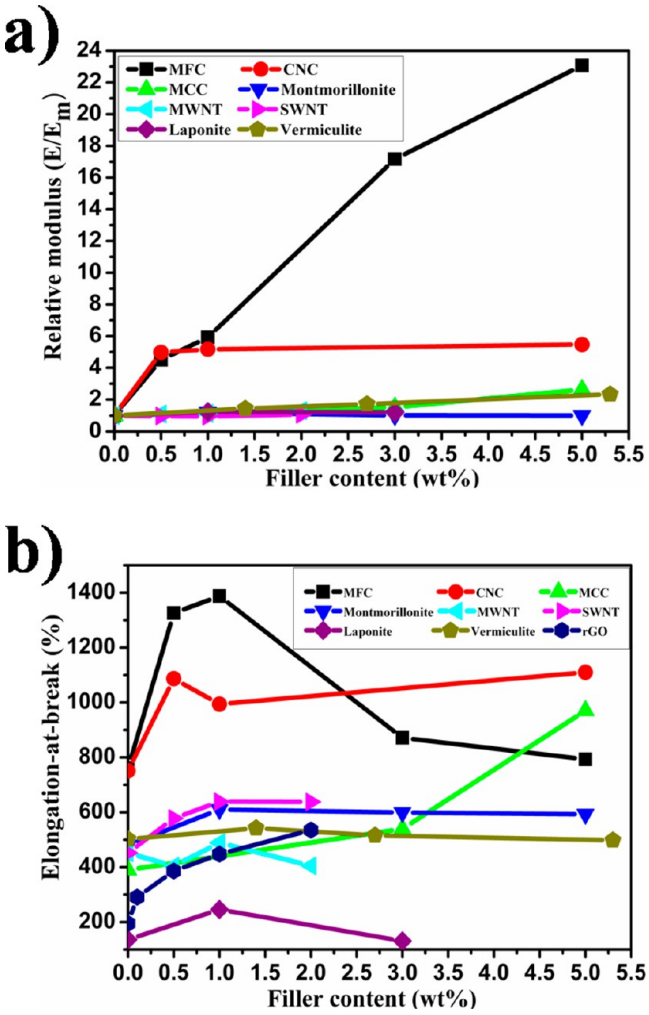

Figure 9. (a) Relative modulus (E/E_m) and (b) elongation-at-break vs filler content for TPU reinforced with MFC (this work), CNC, MCC, montmorillonite, MWNTs, SWNTs, laponite, vermiculite, or rGO. The data for TPU nanocomposites were drawn from this work and the literature.[2,4,5,10,11,60,61]

examined, and the results are shown in Figure 10. Compared with the micrograph of neat TPU (Figure 10a), some pulled-out MFC can be easily identified in the fracture surface of TPU/MFC-1 (Figure 10b). Because of the covalent attachment of the TPU molecules to the stiff surface of MFC and the weblike structure, the pullout of MFC from the TPU matrix requires more energy even at a low content, which contributes to the better mechanical properties. More importantly, the network structure of microfibrillated cellulose can slow down the propagation speed of cracks during tensile fracture. For TPU/MFC-1, some MFC bridges the cracks and forms a networklike structure within the sample (Figure 10c), which plays an important role in the increased tensile strength and elongation-at-break. The pullout of MFC from the TPU matrix allows MFC to bridge cracks when it unravels. As a matter of fact, it is expected that fiber breaking prevails during crack propagation when the adhesion between the fiber and the matrix is too strong.[69−71] The elongation-at-break decreases when the MFC content is higher than 1 wt % because more entanglement exists in the composites and forms aggregation, as shown in Figure 10d. Figure 11 illustrates the failure mechanisms of TPU reinforced with MFC.

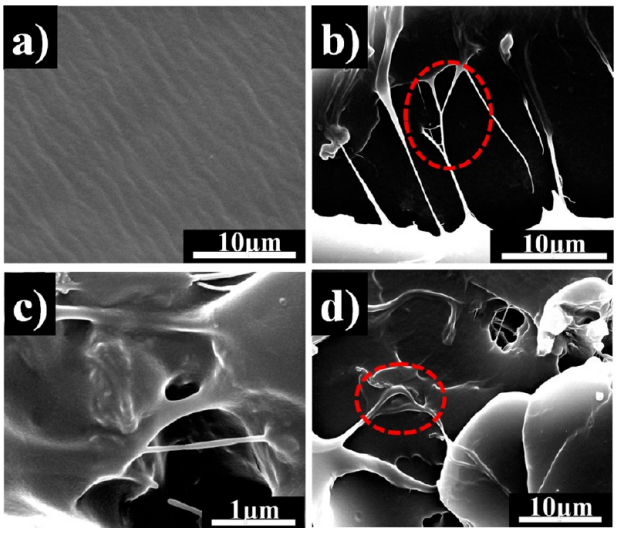

Figure 10. Fracture surfaces of TPU/MFC nanocomposites with different MFC contents. (a) 0 wt % MFC. (b, c) 1 wt % MFC. The region indicated by the ellipse shows the interlocking between fibrils at the fracture surface. (d) 3 wt % MFC. The region indicated by the ellipse shows the entanglement.

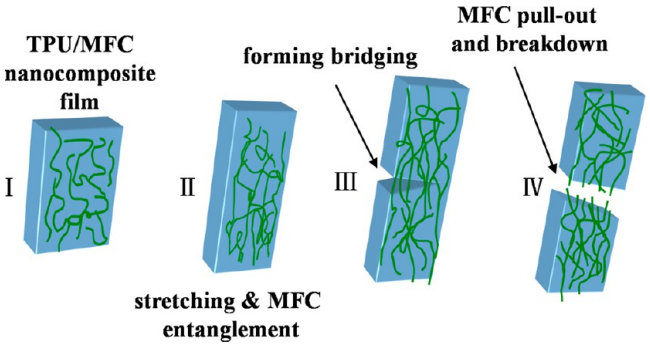

Figure 11. Illustrations of fracture mechanisms in TPU/MFC nanocomposites.

3.6. Optical Properties of TPU/MFC Nanocomposites.

The prepared TPU/MFC nanocomposites show not only much improved mechanical properties but also excellent transparency. Figure 12 shows UV−vis spectra of TPU/MFC

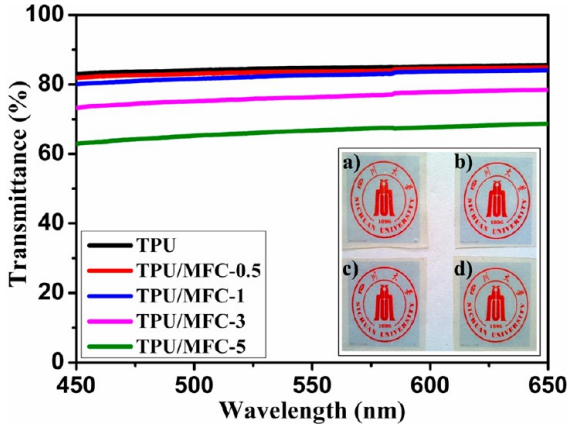

Figure 12. UV−vis spectra of neat TPU and TPU/MFC nanocomposite films. Insets: photos of TPU/MFC nanocomposite films with different MFC loadings: (a) 0, (b) 1, (c) 3, and (d) 5 wt %.

dx.doi.org/10.1021/am4056694 | ACS Appl. Mater. Interfaces 2014, 6, 2497−2507

nanocomposite films with different MFC loadings. The TPU/MFC films containing 0.5 and 1 wt % MFC have light transmittance values of 84.49% and 83.64% at 600 nm, and neat TPU displays a transmittance of 85.17%. The degree of transparency of the TPU/MFC nanocomposite films also reflects the status of dispersion of MFC in the TPU matrix. As shown in the Figure 12 insets, the neat TPU film and the TPU/MFC films with 1 and 3 wt % MFC are nearly optically transparent while the nanocomposite film with 5 wt % MFC is translucent, indicating that MFC achieves a better dispersion even at a relatively high loading. More importantly, this property of these nanocomposite films is advantageous in optical applications where several other nanocomposites (e.g., carbon nanotube, graphene, and clay nanocomposites) cannot be applied because of their lack of transparency.

4. CONCLUSIONS

A series of TPU/MFC nanocomposites have been prepared via in situ polymerization and processed by casting and evaporation. Parts of the presynthesized TPU chains are successfully grafted on the MFC through the reaction between hydroxyl groups on the MFC surfaces and isocyanate groups on the ends of the TPU prepolymer. MFC is strongly associated with the hard segments of TPU through covalent attachment. As a result, good dispersion, the existing network structure in the TPU matrix, and strong interfacial association between MFC and TPU are achieved, which are important to maintain good transparency of the resulting nanocomposites and strengthen the thermoplastic polyurethane without sacrificing the extensibility. Overall we have demonstrated an effective approach for preparing TPU nanocomposites with simultaneously enhanced stiffness and toughness by incorporation of a very small amount of MFC, and the TPU/MFC nanocomposites with excellent stiffness, toughness, thermostability, transparency, and biodegradability may find wider application, especially in optical and bio-related applications, where several other conventional nanocomposites cannot be applied.

■ ASSOCIATED CONTENT

Supporting Information

Optical and SEM images of as-received MFC material and dried MFC after homogenization by the emulsification machine in water and DMF, respectively. This material is available free of charge via the Internet at http://pubs.acs.org.

■ AUTHOR INFORMATION

Corresponding Authors

*E-mail: fengchen@scu.edu.cn. Tel: +86-28-85460690.

*E-mail: qiangfu@scu.edu.cn. Tel/Fax: +86-28-85461795.

Notes

The authors declare no competing financial interest.

■ ACKNOWLEDGMENTS

This work was supported by the National Natural Science Foundation of China (Grants 51173112 and 51121001) and the Special Funds for Major State Basic Research Projects of China (2011CB606006).

■ REFERENCES

(1) Zhao, C.-X.; Zhang, W.-D. Preparation of Waterborne Polyurethane Nanocomposites: Polymerization from Functionalized Hydroxyapatite. *Eur. Polym. J.* **2008**, *44*, 1988−1995.

(2) Tien, Y.; Wei, K. Hydrogen Bonding and Mechanical Properties in Segmented Montmorillonite/Polyurethane Nanocomposites of Different Hard Segment Ratios. *Polymer* **2001**, *42*, 3213−3221.

(3) Johnson, J. R., III; Spikowski, J.; Schiraldi, D. A. Mineralization of Clay/Polymer Aerogels: A Bioinspired Approach to Composite Reinforcement. *ACS Appl. Mater. Interfaces* **2009**, *1*, 1305−1309.

(4) Liff, S. M.; Kumar, N.; McKinley, G. H. High-Performance Elastomeric Nanocomposites via Solvent-Exchange Processing. *Nat. Mater.* **2006**, *6*, 76−83.

(5) Qian, Y.; Lindsay, C. I.; Macosko, C.; Stein, A. Synthesis and Properties of Vermiculite-Reinforced Polyurethane Nanocomposites. *ACS Appl. Mater. Interfaces* **2011**, *3*, 3709−3717.

(6) Zhou, C.-H.; Shen, Z.-F.; Liu, L.-H.; Liu, S.-M. Preparation and Functionality of Clay-Containing Films. *J. Mater. Chem.* **2011**, *21*, 15132−15153.

(7) Huang, Y.-C.; Lin, J.-H.; Tseng, I.; Lo, A.-Y.; Lo, T.-Y.; Yu, H.-P.; Tsai, M.-H.; Whang, W.-T.; Hsu, K.-Y. An in-Situ Fabrication Process for Highly Electrical Conductive Polyimide/MWCNT Composite Films Using 2,6-Diaminoanthraquinone. *Compos. Sci. Technol.* **2013**, *87*, 174−181.

(8) Guo, H.; Minus, M. L.; Jagannathan, S.; Kumar, S. Polyacrylonitrile/Carbon Nanotube Composite Films. *ACS Appl. Mater. Interfaces* **2010**, *2*, 1331−1342.

(9) Kim, J.; Hong, S. M.; Kwak, S.; Seo, Y. Physical Properties of Nanocomposites Prepared by in Situ Polymerization of High-Density Polyethylene on Multiwalled Carbon Nanotubes. *Phys. Chem. Chem. Phys.* **2009**, *11*, 10851−10859.

(10) Xia, H.; Song, M. Preparation and Characterization of Polyurethane−Carbon Nanotube Composites. *Soft Matter* **2005**, *1*, 386−394.

(11) Wang, X.; Hu, Y.; Song, L.; Yang, H.; Xing, W.; Lu, H. In Situ Polymerization of Graphene Nanosheets and Polyurethane with Enhanced Mechanical and Thermal Properties. *J. Mater. Chem.* **2011**, *21*, 4222−4227.

(12) Eichhorn, S.; Dufresne, A.; Aranguren, M.; Marcovich, N.; Capadona, J.; Rowan, S.; Weder, C.; Thielemans, W.; Roman, M.; Renneckar, S. Review: Current International Research into Cellulose Nanofibres and Nanocomposites. *J. Mater. Sci.* **2010**, *45*, 1−33.

(13) Moon, R. J.; Martini, A.; Nairn, J.; Simonsen, J.; Youngblood, J. Cellulose Nanomaterials Review: Structure, Properties and Nanocomposites. *Chem. Soc. Rev.* **2011**, *40*, 3941−3994.

(14) O'Sullivan, A. C. Cellulose: The Structure Slowly Unravels. *Cellulose* **1997**, *4*, 173−207.

(15) Siró, I.; Plackett, D. Microfibrillated Cellulose and New Nanocomposite Materials: A Review. *Cellulose* **2010**, *17*, 459−494.

(16) Klemm, D.; Heublein, B.; Fink, H. P.; Bohn, A. Cellulose: Fascinating Biopolymer and Sustainable Raw Material. *Angew. Chem., Int. Ed.* **2005**, *44*, 3358−3393.

(17) Azizi Samir, M. A. S.; Alloin, F.; Sanchez, J.-Y.; El Kissi, N.; Dufresne, A. Preparation of Cellulose Whiskers Reinforced Nanocomposites from an Organic Medium Suspension. *Macromolecules* **2004**, *37*, 1386−1393.

(18) Zoppe, J. O.; Peresin, M. S.; Habibi, Y.; Venditti, R. A.; Rojas, O. J. Reinforcing Poly(ε-caprolactone) Nanofibers with Cellulose Nanocrystals. *ACS Appl. Mater. Interfaces* **2009**, *1*, 1996−2004.

(19) Qi, H.; Cai, J.; Zhang, L.; Kuga, S. Properties of Films Composed of Cellulose Nanowhiskers and a Cellulose Matrix Regenerated from Alkali/Urea Solution. *Biomacromolecules* **2009**, *10*, 1597−1602.

(20) Siqueira, G.; Abdillahi, H.; Bras, J.; Dufresne, A. High Reinforcing Capability Cellulose Nanocrystals Extracted from *Syngonanthus nitens* (Capim Dourado). *Cellulose* **2010**, *17*, 289−298.

(21) Cao, X.; Xu, C.; Liu, Y.; Chen, Y. Preparation and Properties of Carboxylated Styrene−Butadiene Rubber/Cellulose Nanocrystals Composites. *Carbohydr. Polym.* **2012**, *92*, 69−76.

(22) Goffin, A.-L.; Habibi, Y.; Raquez, J.-M.; Dubois, P. Polyester-Grafted Cellulose Nanowhiskers: A New Approach for Tuning the Microstructure of Immiscible Polyester Blends. *ACS Appl. Mater. Interfaces* **2012**, *4*, 3364−3371.

(23) Morandi, G.; Thielemans, W. Synthesis of Cellulose Nanocrystals Bearing Photocleavable Grafts by ATRP. *Polym. Chem.* **2012**, *3*, 1402−1407.
(24) Khelifa, F.; Habibi, Y.; Leclère, P.; Dubois, P. Convection-Assisted Assembly of Cellulose Nanowhiskers Embedded in an Acrylic Copolymer. *Nanoscale* **2013**, *5*, 1082−1090.
(25) Yang, J.; Han, C.-R.; Duan, J.-F.; Xu, F.; Sun, R.-C. Mechanical and Viscoelastic Properties of Cellulose Nanocrystals Reinforced Poly(ethylene glycol) Nanocomposite Hydrogels. *ACS Appl. Mater. Interfaces* **2013**, *5*, 3199−3207.
(26) Dong, X. M.; Revol, J.-f.; Gray, D. G. Effect of Microcrystallite Preparation Conditions on the Formation of Colloid Crystals of Cellulose. *Cellulose* **1998**, *5*, 19−32.
(27) Roman, M.; Winter, W. T. Effect of Sulfate Groups from Sulfuric Acid Hydrolysis on the Thermal Degradation Behavior of Bacterial Cellulose. *Biomacromolecules* **2004**, *5*, 1671−1677.
(28) Bondeson, D.; Mathew, A.; Oksman, K. Optimization of the Isolation of Nanocrystals from Microcrystalline Cellulose by Acid Hydrolysis. *Cellulose* **2006**, *13*, 171−180.
(29) Henriksson, M.; Henriksson, G.; Berglund, L.; Lindström, T. An Environmentally Friendly Method for Enzyme-Assisted Preparation of Microfibrillated Cellulose (MFC) Nanofibers. *Eur. Polym. J.* **2007**, *43*, 3434−3441.
(30) Li, J.; Wei, X.; Wang, Q.; Chen, J.; Chang, G.; Kong, L.; Su, J.; Liu, Y. Homogeneous Isolation of Nanocellulose from Sugarcane Bagasse by High Pressure Homogenization. *Carbohydr. Polym.* **2012**, *90*, 1609−1613.
(31) Wang, Q. Q.; Zhu, J. Y.; Gleisner, R.; Kuster, T. A.; Baxa, U.; McNeil, S. E. Morphological Development of Cellulose Fibrils of a Bleached Eucalyptus Pulp by Mechanical Fibrillation. *Cellulose* **2012**, *19*, 1631−1643.
(32) Zimmermann, T.; Bordeanu, N.; Strub, E. Properties of Nanofibrillated Cellulose from Different Raw Materials and Its Reinforcement Potential. *Carbohydr. Polym.* **2010**, *79*, 1086−1093.
(33) Isogai, A.; Saito, T.; Fukuzumi, H. TEMPO-Oxidized Cellulose Nanofibers. *Nanoscale* **2011**, *3*, 71−85.
(34) Stenstad, P.; Andresen, M.; Tanem, B. S.; Stenius, P. Chemical Surface Modifications of Microfibrillated Cellulose. *Cellulose* **2008**, *15*, 35−45.
(35) Svagan, A. J.; Samir, M. A.; Berglund, L. A. Biomimetic Foams of High Mechanical Performance Based on Nanostructured Cell Walls Reinforced by Native Cellulose Nanofibrils. *Adv. Mater.* **2008**, *20*, 1263−1269.
(36) Tingaut, P.; Zimmermann, T.; Sèbe, G. Cellulose Nanocrystals and Microfibrillated Cellulose as Building Blocks for the Design of Hierarchical Functional Materials. *J. Mater. Chem.* **2012**, *22*, 20105−20111.
(37) Henriksson, M.; Berglund, L. A.; Isaksson, P.; Lindstrom, T.; Nishino, T. Cellulose Nanopaper Structures of High Toughness. *Biomacromolecules* **2008**, *9*, 1579−1585.
(38) Liimatainen, H.; Ezekiel, N.; Sliz, R.; Ohenoja, K.; Sirviö, J. A.; Berglund, L.; Hormi, O.; Niinimäki, J. High Strength Nanocellulose−Talc Hybrid Barrier Films. *ACS Appl. Mater. Interfaces* **2013**, *5*, 13412−13418.
(39) Pääkkö, M.; Vapaavuori, J.; Silvennoinen, R.; Kosonen, H.; Ankerfors, M.; Lindström, T.; Berglund, L. A.; Ikkala, O. Long and Entangled Native Cellulose I Nanofibers Allow Flexible Aerogels and Hierarchically Porous Templates for Functionalities. *Soft Matter* **2008**, *4*, 2492−2499.
(40) Olsson, R. T.; Samir, M. A.; Salazar-Alvarez, G.; Belova, L.; Ström, V.; Berglund, L. A.; Ikkala, O.; Nogues, J.; Gedde, U. W. Making Flexible Magnetic Aerogels and Stiff Magnetic Nanopaper Using Cellulose Nanofibrils as Templates. *Nat. Nanotechnol.* **2010**, *5*, 584−588.
(41) Hsieh, M.-C.; Kim, C.; Nogi, M.; Suganuma, K. Electrically Conductive Lines on Cellulose Nanopaper for Flexible Electrical Devices. *Nanoscale* **2013**, *5*, 9289−9295.
(42) Shi, Z.; Phillips, G. O.; Yang, G. Nanocellulose Electroconductive Composites. *Nanoscale* **2013**, *5*, 3194−3201.
(43) Yano, H.; Sugiyama, J.; Nakagaito, A. N.; Nogi, M.; Matsuura, T.; Hikita, M.; Handa, K. Optically Transparent Composites Reinforced with Networks of Bacterial Nanofibers. *Adv. Mater.* **2005**, *17*, 153−155.
(44) Aulin, C.; Karabulut, E.; Tran, A.; Wågberg, L.; Lindström, T. Transparent Nanocellulosic Multilayer Thin Films on Polylactic Acid with Tunable Gas Barrier Properties. *ACS Appl. Mater. Interfaces* **2013**, *5*, 7352−7359.
(45) Lee, K.-Y.; Tammelin, T.; Schulfter, K.; Kiiskinen, H.; Samela, J.; Bismarck, A. High Performance Cellulose Nanocomposites: Comparing the Reinforcing Ability of Bacterial Cellulose and Nanofibrillated Cellulose. *ACS Appl. Mater. Interfaces* **2012**, *4*, 4078−4086.
(46) Nakagaito, A.; Iwamoto, S.; Yano, H. Bacterial Cellulose: The Ultimate Nano-Scalar Cellulose Morphology for the Production of High-Strength Composites. *Appl. Phys. A: Mater. Sci. Process.* **2005**, *80*, 93−97.
(47) Lönnberg, H.; Larsson, K.; Lindström, T.; Hult, A.; Malmström, E. Synthesis of Polycaprolactone-Grafted Microfibrillated Cellulose for Use in Novel Bionanocomposites—Influence of the Graft Length on the Mechanical Properties. *ACS Appl. Mater. Interfaces* **2011**, *3*, 1426−1433.
(48) Siqueira, G.; Bras, J.; Dufresne, A. Cellulose Whiskers versus Microfibrils: Influence of the Nature of the Nanoparticle and Its Surface Functionalization on the Thermal and Mechanical Properties of Nanocomposites. *Biomacromolecules* **2009**, *10*, 425−432.
(49) Javadi, A.; Zheng, Q.; Payen, F.; Javadi, A.; Altin, Y.; Cai, Z.; Sabo, R.; Gong, S. Polyvinyl Alcohol−Cellulose Nanofibrils−Graphene Oxide Hybrid Organic Aerogels. *ACS Appl. Mater. Interfaces* **2013**, *5*, 5969−5975.
(50) Cheng, Q.; Wang, S.; Rials, T. G. Poly(vinyl alcohol) Nanocomposites Reinforced with Cellulose Fibrils Isolated by High Intensity Ultrasonication. *Composites, Part A* **2009**, *40*, 218−224.
(51) Fujisawa, S.; Ikeuchi, T.; Takeuchi, M.; Saito, T.; Isogai, A. Superior Reinforcement Effect of TEMPO-Oxidized Cellulose Nanofibrils in Polystyrene Matrix: Optical, Thermal, and Mechanical Studies. *Biomacromolecules* **2012**, *13*, 2188−2194.
(52) Wang, C. B.; Cooper, S. L. Morphology and Properties of Segmented Polyether Polyurethaneureas. *Macromolecules* **1983**, *16*, 775−786.
(53) Miller, J. A.; Lin, S. B.; Hwang, K. K.; Wu, K.; Gibson, P.; Cooper, S. L. Properties of Polyether−Polyurethane Block Copolymers: Effects of Hard Segment Length Distribution. *Macromolecules* **1985**, *18*, 32−44.
(54) Koberstein, J. T.; Russell, T. P. Simultaneous SAXS−DSC Study of Multiple Endothermic Behavior in Polyether-Based Polyurethane Block Copolymers. *Macromolecules* **1986**, *19*, 714−720.
(55) Martin, D. J.; Meijs, G. F.; Renwick, G. M.; Mccarthy, S. J.; Gunatillake, P. A. The Effect of Average Soft Segment Length on Morphology and Properties of a Series of Polyurethane Elastomers. I. Characterization of the Series. *J. Appl. Polym. Sci.* **1996**, *62*, 1377−1386.
(56) Martin, D. J.; Meijs, G. F.; Gunatillake, P. A.; Yozghatlian, S. P.; Renwick, G. M. The Influence of Composition Ratio on the Morphology of Biomedical Polyurethanes. *J. Appl. Polym. Sci.* **1999**, *71*, 937−952.
(57) Yeh, F.; Hsiao, B. S.; Sauer, B. B.; Michel, S.; Siesler, H. W. In-Situ Studies of Structure Development During Deformation of a Segmented Poly(urethane−urea) Elastomer. *Macromolecules* **2003**, *36*, 1940−1954.
(58) Marcovich, N.; Auad, M.; Bellesi, N.; Nutt, S.; Aranguren, M. Cellulose Micro/Nanocrystals Reinforced Polyurethane. *J. Mater. Res.* **2006**, *21*, 870−881.
(59) Auad, M. L.; Mosiewicki, M. A.; Richardson, T.; Aranguren, M. I.; Marcovich, N. E. Nanocomposites Made from Cellulose Nanocrystals and Tailored Segmented Polyurethanes. *J. Appl. Polym. Sci.* **2010**, *115*, 1215−1225.
(60) Pei, A.; Malho, J.-M.; Ruokolainen, J.; Zhou, Q.; Berglund, L. A. Strong Nanocomposite Reinforcement Effects in Polyurethane

Elastomer with Low Volume Fraction of Cellulose Nanocrystals. *Macromolecules* **2011**, *44*, 4422−4427.
(61) Wu, Q.; Henriksson, M.; Liu, X.; Berglund, L. A. A High Strength Nanocomposite Based on Microcrystalline Cellulose and Polyurethane. *Biomacromolecules* **2007**, *8*, 3687−3692.
(62) Özgür Seydibeyoğlu, M.; Oksman, K. Novel Nanocomposites Based on Polyurethane and Micro Fibrillated Cellulose. *Compos. Sci. Technol.* **2008**, *68*, 908−914.
(63) Auad, M. L.; Richardson, T.; Orts, W. J.; Medeiros, E. S.; Mattoso, L. H.; Mosiewicki, M. A.; Marcovich, N. E.; Aranguren, M. I. Polyaniline-Modified Cellulose Nanofibrils as Reinforcement of a Smart Polyurethane. *Polym. Int.* **2011**, *60*, 743−750.
(64) Petrović, Z. S.; Zavargo, Z.; Flyn, J. H.; Macknight, W. J. Thermal Degradation of Segmented Polyurethanes. *J. Appl. Polym. Sci.* **1994**, *51*, 1087−1095.
(65) McNally, T.; Pötschke, P.; Halley, P.; Murphy, M.; Martin, D.; Bell, S. E.; Brennan, G. P.; Bein, D.; Lemoine, P.; Quinn, J. P. Polyethylene Multiwalled Carbon Nanotube Composites. *Polymer* **2005**, *46*, 8222−8232.
(66) Zhao, X.; Zhang, Q.; Chen, D.; Lu, P. Enhanced Mechanical Properties of Graphene-Based Poly(vinyl alcohol) Composites. *Macromolecules* **2010**, *43*, 2357−2363.
(67) Prachum, Y.; Strauss, A.; Helmuth, R.; Kiatkamjornwong, S. The Physical and Mechanical Properties of β-Nucleated Polypropylene/Montmorillonite Nanocomposites. *J. Appl. Polym. Sci.* **2011**, *122*, 1066−1076.
(68) Li, Z.; Young, R. J.; Kinloch, I. A. Interfacial Stress Transfer in Graphene Oxide Nanocomposites. *ACS Appl. Mater. Interfaces* **2013**, *5*, 456−463.
(69) Qian, D.; Dickey, E. C.; Andrews, R.; Rantell, T. Load Transfer and Deformation Mechanisms in Carbon Nanotube−Polystyrene Composites. *Appl. Phys. Lett.* **2000**, *76*, 2868.
(70) Ayatollahi, M.; Shadlou, S.; Shokrieh, M. Correlation between Aspect Ratio of MWCNTs and Mixed Mode Fracture of Epoxy Based Nanocomposites. *Mater. Sci. Eng., A* **2011**, *528*, 6173−6178.
(71) Gong, G.; Pyo, J.; Mathew, A. P.; Oksman, K. Tensile Behavior, Morphology and Viscoelastic Analysis of Cellulose Nanofiber-Reinforced (CNF) Polyvinyl Acetate (PVAc). *Composites, Part A* **2011**, *42*, 1275−1282.